Size distribution and mixing state of refractory black carbon aerosol from a coastal city in South China

Wang, Qiyuan; Huang, Ru-Jin; Zhao, Zhuzi; Zhang, Ningning; Wang, Yichen; Ni, Haiyan; Tie, Xuexi; Han, Yongming; Zhuang, Mazhan; Wang, Meng

Published in:
Atmospheric research

DOI:
10.1016/j.atmosres.2016.06.022

Atmospheric Research 181 (2016) 163–171

Contents lists available at ScienceDirect

Atmospheric Research

journal homepage: www.elsevier.com/locate/atmosres

Size distribution and mixing state of refractory black carbon aerosol from a coastal city in South China

Qiyuan Wang [a], Ru-Jin Huang [a,b,c,*], Zhuzi Zhao [a], Ningning Zhang [a], Yichen Wang [a], Haiyan Ni [a], Xuexi Tie [a,d], Yongming Han [a,e], Mazhan Zhuang [f], Meng Wang [a], Jieru Zhang [f], Xuemin Zhang [f], Uli Dusek [g], Junji Cao [a,e,*]

[a] Key Laboratory of Aerosol Chemistry and Physics, SKLLQG, Institute of Earth Environment, Chinese Academy of Sciences, Xi'an 710061, China
[b] Laboratory of Atmospheric Chemistry, Paul Scherrer Institute (PSI), 5232 Villigen, Switzerland
[c] Centre for Atmospheric and Marine Sciences, Xiamen Huaxia University, Xiamen 361024, China
[d] Center for Excellence in Urban Atmospheric Environment, Institute of Urban Environment, Chinese Academy of Sciences, Xiamen 361021, China
[e] Institute of Global Environmental Change, Xi'an Jiaotong University, Xi'an 710049, China
[f] Xiamen Environmental Monitoring Central Station, Xiamen 361012, China
[g] Centre for Isotope Research (CIO), Energy and Sustainability Research Institute Groningen (ESRIG), University of Groningen, The Netherlands

ARTICLE INFO

Article history:
Received 13 March 2016
Received in revised form 15 June 2016
Accepted 24 June 2016
Available online 25 June 2016

Keywords:
Refractory black carbon
Potential sources
Size distributions
Mixing state

ABSTRACT

An intensive measurement campaign was conducted in the coastal city of Xiamen, China to investigate the size distribution and mixing state of the refractory black carbon (rBC) aerosol. The average rBC concentration for the campaign, measured with a ground-based single particle soot photometer (SP2), was 2.3 ± 1.7 μg m^{-3}, which accounted for ~4.3% of the $PM_{2.5}$ mass. A potential source contribution function model indicated that emissions from coastal cities to the southwest were the most important source for the rBC and that shipping traffic was another likely source. The mass size distribution of the rBC particles was mono-modal and approximately lognormal, with a mass median diameter (MMD) of ~185 nm. Larger MMDs (~195 nm) occurred during polluted conditions compared with non-polluted times (~175 nm) due to stronger biomass burning activities during pollution episodes. Uncoated or thinly-coated particles composed the bulk of the rBC aerosol, and on average ~31% of the rBC was internally-mixed or thickly-coated. A positive matrix factorization model showed that organic materials were the predominant component of the rBC coatings and that mixing with nitrate increased during pollution conditions. These findings should lead to improvements in the parameterizations used to model the radiative effects of rBC.

1. Introduction

The black carbon (BC) aerosol plays an important role in the Earth's climate system, mainly due to its strong absorption of solar radiation at visible wavelengths both in the atmosphere (e.g., Ramana et al., 2010; Das and Jayaraman, 2011) and after the particles are deposited onto snow (e.g., Xu et al., 2009; Hadley and Kirchstetter, 2012). BC is a by-product of the incomplete combustion of fossil fuels and the burning of biomass and other fuels (Bond et al., 2013). The global emission of BC in 2007 was estimated to be ~8.7 Tg yr^{-1}, and of this 1.6 Tg yr^{-1} was from industry, 2.8 Tg yr^{-1} from residential/commercial sectors, and 1.5 Tg yr^{-1} from transportation (Wang, 2015). The Fifth Assessment Report of the Intergovernmental Panel on Climate Change (IPCC) suggests that the direct radiative forcing of BC aerosol is +0.6 W m^{-2}: +0.4 W m^{-2} of that is due to emissions from the burning of fossil fuels and biofuels (IPCC, 2013). Bond et al. (2013) estimated a larger BC direct radiative forcing effect of +0.71 W m^{-2}, with +0.51 W m^{-2} from fossil and biofuel emissions and +0.2 W m^{-2} from biomass burning. More generally, in addition to carbon dioxide and methane, BC is considered one of the most important chemical species for climate warming. From a different perspective, BC is an important component of air pollution because the particles can impair visibility (Wang et al., 2013), and it also has been suggested that BC adversely affects human health, mainly through direct inhalation. The inhaled particles can damage the vascular system and cause both cardiopulmonary and respiratory disease (Cornell et al., 2012; Heal et al., 2012).

Although the BC aerosol is almost chemically inert in the atmosphere (Dumka et al., 2010), it can act as a carrier, and heterogeneous surface reactions can change the particles' chemical composition,

* Corresponding authors at: Key Laboratory of Aerosol Chemistry and Physics, SKLLQG, Institute of Earth Environment, Chinese Academy of Sciences, Xi'an 710061, China.
E-mail addresses: rujin.huang@ieecas.cn (R.-J. Huang), cao@loess.llqg.ac.cn (J. Cao).

http://dx.doi.org/10.1016/j.atmosres.2016.06.022
0169-8095/

morphology and hygroscopicity (Zhang and Zhang, 2005). The presence of internally-mixed, non-BC material (e.g., sulfates, nitrates or organic substances) is thought to increase the light absorption properties of BC particles through a "lensing effect" (e.g, Wang et al., 2014a; Liu et al., 2015). Moreover, increases in the size and hydrophilicity of BC particles can enhance their removal through precipitation scavenging (Liu et al., 2013), and this in turn, has implications for climate forcing. In this regard, the average atmospheric lifetime of BC aerosol is about several days to weeks (Cape et al., 2012), making it a potential candidate for short time-scale mitigation of global warming (Ramanathan and Carmichael, 2008).

China is one of the world's largest contributors to the BC aerosol (Ni et al., 2014), and even though the characteristics of BC aerosol in various Chinese cities have been studied over the past several decades (e.g., Wu et al., 2013; Feng et al., 2014; Cao et al., 2015), the information on ambient BC size distributions and mixing state is more limited than that on total BC mass concentrations. For example, Cheng et al. (2006) investigated the mixing state of BC and non-light-absorbing aerosol components at Xinken in Pearl River Delta of China, and they found that the BC mixing state varied with the wind direction and wind strength. When airflow was controlled by local winds the mixing state varied diurnally; that is, during the daytime the winds were light and the BC was mainly internally mixed due to the effects of local pollution, but at night the externally mixed BC mass ratio increased to an average of 53%. At present, estimates of BC radiative forcing still remain highly uncertain, and the information on size and mixing state of BC aerosol would not only benefit the climate modelers but also support the development of policies and regulations that target both climate change and air pollution.

Although BC is important for climate and air quality, there is no agreement on the terminology and definitions that deal with all aspects of the properties, measurement methods, and related uncertainties of this material (Petzold et al., 2013). Here, we use the designation refractory black carbon (rBC) instead of BC because the measurements were made using an incandescence method rather than the more commonly used thermal-optical or light-absorption methods (Bond et al., 2013; Petzold et al., 2013). Previous studies have shown that BC mass concentrations measured by these different techniques are both consistent and traceable (Kondo et al., 2011). In this study, we deployed a single particle soot photometer (SP2) to measure rBC and an aerosol chemical speciation monitor (ACSM) to measure the concentrations of selected chemical species during spring in Xiamen, China. The objectives of the study were (1) to determine the rBC mass concentrations and identify likely source regions, (2) to characterize the rBC size distributions under different pollution levels, and (3) to investigate the relationships between thickly-coated rBC particles and non-rBC materials. The results obtained with the SP2 contribute to our understanding of the physical and chemical characteristics rBC particles under different pollution levels, and that information should lead to improvements in the parameterizations needed for models of rBC radiative effects and possibly in control measures.

2. Experimental

2.1. Measurement site

The physical and chemical properties of rBC particles were studied in samples collected at a coastal urban site on the northwestern side of Xiamen Island (Fig. S1). The sampling site was located on the rooftop of a building of the Power Supply Bureau (24.52°N, 118.09°E, ~10 m above ground level), which is a state-controlled air-sampling site established by Xiamen Environmental Protection Bureau. Intensive measurements were carried out from 1 to 31 March 2013 using an SP2 and an ACSM. The sampling site is surrounded by commercial and residential districts, and no major industrial sources are located nearby. To the south is the Huli road (~100 m), where the traffic is heavy while to the west is the Huachang road (~170 m), which has less traffic. This sampling site may be considered generally representative of urban conditions in Xiamen.

2.2. Single particle soot photometer

The mass, size distribution, and mixing state of rBC particles were characterized using a commercially available SP2 instrument (Droplet Measurement Technology, Boulder, CO, USA). As described previously (e.g, Gao et al., 2007; Schwarz et al., 2015), the SP2 measurements are based on a laser-induced incandescence method, which uses an intracavity Nd:YAG laser ($\lambda = 1064$ nm) to heat rBC-containing particles to their boiling point (~4000 K; Schwarz et al., 2006). The refractory mass of each particle is quantified by detecting the emission of thermal radiation. The SP2 has two incandescence channels (broad/narrow) and two scattering channels, consisting of photomultiplier tubes (PMTs) and avalanche photodiodes (APDs), respectively. The incandescence channel signal was used to determine the rBC mass after calibration with standard fullerene soot (Lot F12S011, Alfa Aesar, Inc., Ward Hill, MA, USA). The scattering channel signal was calibrated with different sizes of monodisperse polystyrene latex (PSL) spheres. To verify the stability of the SP2 for the rBC measurements, the laser intensity was monitored by analyzing 269 nm diameter PSL spheres about every three days throughout the experiment (Schwarz et al., 2010), and the results showed that the laser intensity was stable (see Fig. S2). More details concerning the SP2 calibration procedures may be found in our previous publication (Wang et al., 2014b).

The rBC mass is proportional to the SP2 incandescence signal, and it is not sensitive to either the particle's morphology or mixing state (Cross et al., 2010). The total uncertainty of the SP2 measurements is ~20%. The concentrations of rBC are reported for standard temperature and pressure (273.15 K, 1013.25 mbar). The measured atmospheric rBC masses were converted to mass equivalent diameters (MEDs), assuming the particles were solid spheres with a density of 2.0 g cm^{-3} (Slowik et al., 2004). The rBC size as used here refers to the MED of the "core", and it does not include the contributions of non-rBC material to the particle diameter.

Compared with filter-based observations (e.g., Han et al., 2010; Cao et al., 2013; Zhu et al., 2014), measurements made with the SP2 have an important advantage–the ability to determine the mixing state of the rBC particles (e.g., Perring et al., 2011; Laborde et al., 2013). Often rBC particles in the atmosphere are internally-mixed with non-rBC materials, and this commonly referred to as the "coated state". Coated rBC particles can be seen in the transmission electron microscopy images in Fig. 8 of Li et al. (2011). When the SP2 laser beam heats an internally-mixed rBC particle, the coating vaporizes, causing the peak of the scattering signal to decrease before the onset of the incandescence signal. The lagtime between the peak of scattering signal and the peak of incandescence signal can be used to characterize the coating state (Schwarz et al., 2006). In this study, the frequency distribution of lagtimes displayed a bimodal distribution with ~2 μs separating two distinct populations (Fig. 1); this is similar to the two populations found by Moteki et al. (2007) who investigated the mixing state of rBC particles collected with an aircraft flown over the western Pacific. The rBC particles with an incandescence lagtime >2 μs were considered to have substantial coatings and by inference be thickly-coated while lagtimes <2 μs represented uncoated or thinly-coated particles.

The degree of rBC mixing state is expressed here as the number fraction of thickly-coated rBC (f_{BC}) particles, which is calculated as the ratio between the number of thickly-coated rBC particles and total number of rBC particles. Due to the noisiness in the measurements for small particles and the saturation in the scattering measurements for large particles, the mixing state was determined for rBC cores between ~70–280 nm MED. This is not a major limitation in the data because that size range constitutes a large majority of rBC particle population (e.g., Huang et al., 2012; Wang et al., 2015a).

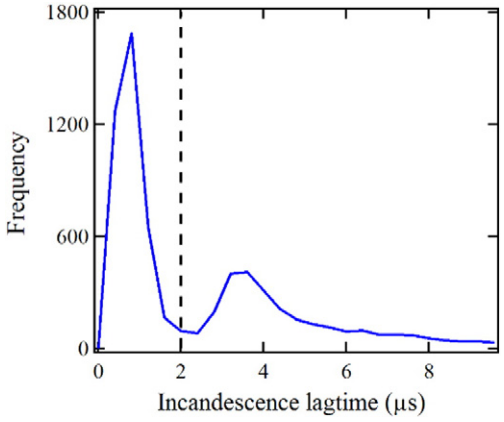

Fig. 1. Histogram of the incandescence lagtimes for ~7000 arbitrary-selected ambient rBC particles during the campaign. The vertical dashed line shows the lagtime of 2 μs which can be used to distinguish thickly-coated rBC particles from uncoated or thinly-coated rBC.

2.3. Aerosol chemical measurements

The mass concentrations of non-refractory PM_1 species (e.g., organics, sulfate, nitrate, ammonium, and chloride) were measured with the use of an aerosol chemical speciation monitor (ACSM, Aerodyne Research Inc., Billerica, MA) that was operated in parallel with the SP2 measurements. Ambient air was drawn into the ACSM at a flow rate of 3 L min^{-1}. The atmospheric particles were dried with a Nafion® dryer (MD-110-48S; Perma Pure, Inc., Lakewood, NJ, USA) before entering the ACSM to avoid water condensation in the sampling line, which would affect the particle collection efficiency (Middlebrook et al., 2012). Detailed descriptions of the operating principles and calibration procedures of ACSM are available elsewhere (Ng et al., 2011). Briefly, the ACSM focuses individual particles (~40–1000 nm vacuum aerodynamic diameter, VAD) into a beam through a critical orifice (100 μm diameter) at a rate of ~0.1 L min^{-1} under vacuum. Then the non-refractory components of the particle beam are vaporized on a hot surface (~600 °C), ionized with 70 eV electrons, and finally the mass fragments analyzed with a quadrupole mass spectrometer. The chemically-speciated, non-refractory aerosol mass loadings are then extracted from the mass spectra. The ACSM response factor (RF) was calculated with the use of monodisperse 300 nm ammonium nitrate particles that were generated using an atomizer (Model 9302, TSI Inc., Shoreview, MN, USA) and a differential mobility analyzer (Model 3080, TSI Inc.). A range of ammonium nitrate concentrations from 0 to 25 μg m^{-3} was used for this purpose, which was produced by diluting the generated aerosol. The relative ionization efficiency for ammonium was directly determined from the ammonium nitrate calibration.

2.4. Complementary measurements

Hourly mass concentrations of $PM_{2.5}$ were measured using a micro-oscillating balance method (TEOM®1405-DF; Thermo Scientific, Waltham, MA, USA). Hourly-average mixing ratios of nitrogen oxides ($NOx = NO_2 + NO$) and ozone (O_3) were obtained through measurements made by a chemiluminescence method (Model 42i Nitrogen Oxide Analyzer, Thermo Scientific) and a UV photometric method (Model 49i Ozone Analyzer, Thermo Scientific), respectively. Wind speed and wind direction were measured every minute with the use of an automatic weather station (MAWS201, Vaisala, Vantaa, Finland) configured with a wind sensor (Vaisala Model QMW101-M2).

3. Results and discussion

3.1. rBC concentrations and potential sources

Time-series plots of the hourly-averaged mass concentrations of rBC and $PM_{2.5}$ for the entire campaign are shown in Fig. 2. The hourly $PM_{2.5}$ mass concentrations varied widely, ranging from 5 to 168 μg m^{-3} with a mean value of 54 μg m^{-3} and a standard deviation (SD) of 25 μg m^{-3}. Although the average value was less than the China National Ambient Air Quality Grade II Standard for daily $PM_{2.5}$ mass concentrations (75 μg m^{-3}, GB3095-2012), ~20% of the samples exceeded that value and so were considered to be more-or-less representative of polluted conditions while the rest were assumed to be more indicative of non-polluted periods. The rBC mass concentrations ranged from 0.3 to 11.3 μg m^{-3}, with an average of 2.3 ± 1.7 μg m^{-3}, which accounted for ~4.3% of $PM_{2.5}$ mass. For the polluted samples, the average rBC concentration was 4.1 ± 2.0 μg m^{-3}, which was higher by a factor of ~2 than the non-polluted samples (2.0 ± 1.4 μg m^{-3}). Compared with SP2-based measurements made at other Chinese cities (see Table 1), the overall average rBC value at Xiamen was lower than Beijing (5.5 μg m^{-3}, Wu et al., 2016), Shanghai (3.2 μg m^{-3}, Gong et al., 2016), Xi'an (8.8 μg m^{-3}, Wang et al., 2014a), and Shenzhen (4.1 μg m^{-3}, Huang et al., 2012). However, the SP2-based rBC mass loadings at Xiamen were higher than similar measurements made in several other cities around the world, including Paris (0.9 μg m^{-3}, Laborde et al., 2013) and London (1.3 μg m^{-3}, Liu et al., 2014).

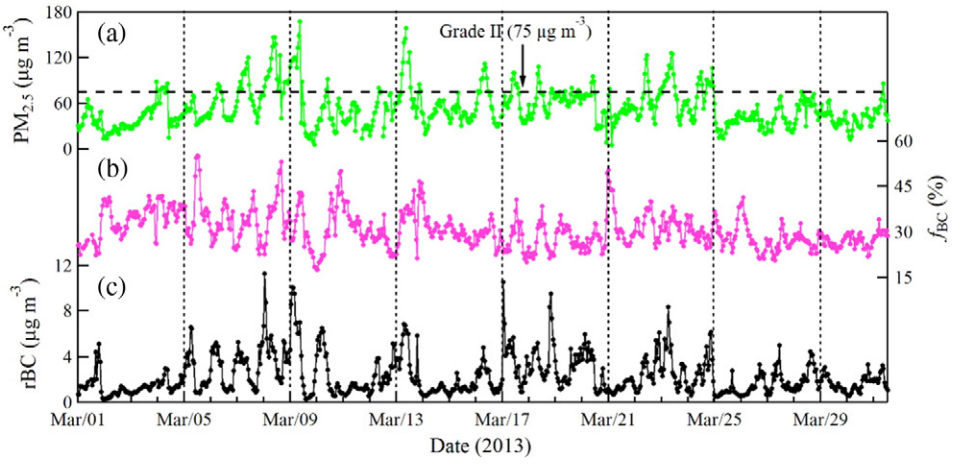

Fig. 2. Time-series plots of hourly-averaged (a) $PM_{2.5}$ mass concentrations, (b) number fractions of thickly-coated rBC (f_{BC}), and (c) refractory black carbon (rBC) mass concentrations. The horizontal dashed line shows the Grade II standard value for daily $PM_{2.5}$ concentration (75 μg m^{-3}) promulgated as the China National Ambient Air Quality Standard (GB3095-2012).

Table 1
Average refractory black carbon (rBC) concentrations at selected locations.

Location	Observation period	rBC (μg m^{-3})	Reference
Xiamen, China	Mar. 2013	2.3 ± 1.7	This study
	Polluted periods	4.1 ± 2.0	
	Non-polluted periods	2.0 ± 1.4	
Beijing, China	Jan. 2013	5.5	Wu et al. (2016)
Shanghai, China	Dec. 2013	3.2	Gong et al. (2016)
Xi'an, China	Dec. 2012–Jan. 2013	8.8 ± 7.3	Wang et al. (2014a)
Shenzhen, China	Jan. 2010	4.1 ± 3.8	Huang et al. (2012)
Paris, France	Jan.–Feb. 2010	0.9 ± 0.7	Laborde et al. (2013)
London, England	Jan.–Feb. and Jul.–Aug. 2012	1.3 ± 1.1	Liu et al. (2014)

Fig. 3 shows the diurnal variations in the rBC concentrations and wind speed averaged over the campaign. The rBC concentrations typically exhibited two peaks per day, and these can be explained by the combined influences of human activities and meteorological conditions. The rBC concentrations showed their first and largest peak value (3.3 μg m^{-3}) in the early morning ~07:00 local standard time (LST–all time references that follow are given in LST), and that was followed by a sharp decrease to a minimum value (1.6–1.9 μg m^{-3}) in the afternoon around 12:00–17:00. The rBC concentrations then increased to a secondary peak value (2.6 μg m^{-3}) in the evening at ~19:00 and then slowly decreased to a minimum (1.9–2.1 μg m^{-3}) at night around 23:00–24:00, similar to what has been observed at the Chinese coastal city of Shenzhen (Huang et al., 2012). After midnight, the rBC loadings were relatively stable at ~2.7 μg m^{-3} until the early morning; that is, before about 06:00.

The elevated rBC concentrations in the morning and evening can be explained by increases in local anthropogenic emissions, especially those from rush-hour traffic. Those impacts presumably were exacerbated by low boundary-layer heights, which led to the near-surface accumulation of pollutants. With increases in solar heating during the day, the depths of the boundary layer and wind speeds both tended to increase (see Fig. 3b), and those meteorological effects led to a dilution of the atmospheric aerosols and as a result lower rBC loadings in the afternoon. The slight decrease in rBC at night between 20:00 and 24:00 may be attributed to relatively strong winds from the northeast at night (Fig. S3). There are no strong rBC emission sources in that direction from the site, and this explanation is also consistent with the source analysis discussed below.

A potential source contribution function (PSCF) model was used to identify the likely source regions for the rBC aerosol at Xiamen, and it was based on three-day trajectories calculated backwards in time for arrival heights of 20, 100, and 500 m above ground. The trajectories were calculated hourly using the hybrid single-particle Lagrangian integrated (HYSPLIT) model (Draxler and Rolph, 2003) which was driven by full vertical dynamics and gridded meteorological data (Global Data Assimilation System; GDAS1, http://ready.arl.noaa.gov/HYSPLIT.php). Each arrival height was retrieved for each of 744 backward trajectories. Fig. 4 (a–c) shows that the trajectories for different arrival heights exhibited similar patterns, suggesting that the air masses can be considered well-mixed from 20 to 500 m.

For the PSCF, the geographic area covered by the trajectories were divided into 3996 grid cells of 0.5° latitude × 0.5° longitude so that there were 54,312 endpoints / 3996 cells or ~14 trajectory endpoints per cell on average. An inherent assumption for the PSCF is that if a source is located within a single geographic grid cell (i, j), air parcels passing over that location will accumulate particles that will then be transported along the trajectory path to the receptor site. Although the PSCF is a useful model for locating potential source regions (e.g., Zhang et al., 2013; Wang et al., 2015b), a limitation of the method is that grid cells can have the same PSCF values when the sample concentrations at the receptor site are either much higher or only slightly higher than the criterion value, which is usually set as the arithmetic mean. This limitation may result in difficulties in distinguishing moderate sources from strong ones, and to compensate, the PSCF results for our study were calculated using the 75th percentile of all the data (3.3 μg m^{-3}) as the criterion value. Indeed, a study by Cheng and Lin (2001) showed that the use of a higher criterion value than the mean could improve the resolution of PSCF source identifications.

Fig. 4 (d–f) shows that the PSCF results were similar for all arrival heights, and that most important potential source region for rBC was to the southwest of Xiamen–that area includes the coastal cities of Shantou and Shanwei where rBC emissions are known to be strong (Zhang et al., 2009). We would also hasten to note that in addition to the influences from these cities, there are possible maritime contributions to rBC due to the heavy commercial shipping traffic in the coastal waters. Previous studies have shown that emissions from ships can be the most important source for rBC over some oceanic regions (Lack and Corbett, 2012).

3.2. rBC core mass size distributions

The size distribution of rBC particles is an important determinant of the aerosols' light absorption characteristics (Reddington et al., 2013), and Fig. 5a shows the mass size distribution of rBC averaged over the entire campaign. A mono-modal lognormal size-distribution was found for the mass-equivalent diameters of the rBC cores; the mass median diameter (MMD) for the ensemble of all samples was ~185 nm, and the geometric standard deviation (σ_{gc}) was 0.47. This MMD value is considerably lower than those obtained with SP2s deployed in Shenzhen (210 nm, Huang et al., 2012) or Xi'an (205 nm, Wang et al.,

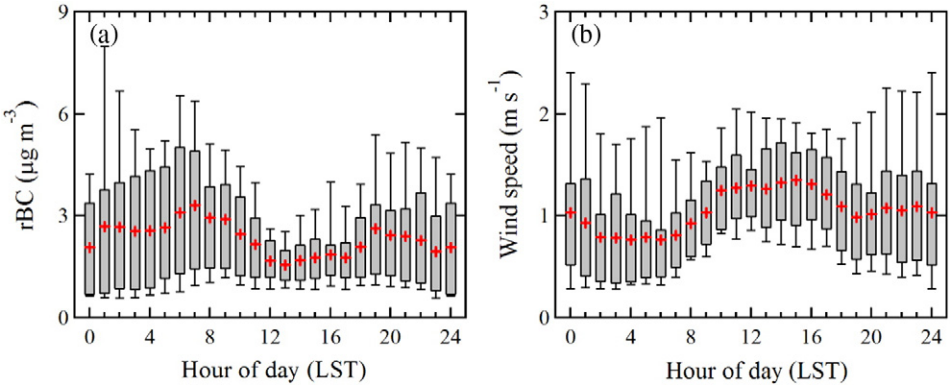

Fig. 3. (a) Diurnal variations of refractory black carbon (rBC) mass concentrations and (b) wind speeds averaged over the campaign. In each panel, the lower and upper edges of the boxes denote the 25% and 75% percentiles, respectively. The red crosses indicate the mean values and vertical bars ("whiskers") show the 10th and 90th percentiles. LST stands for local standard time.

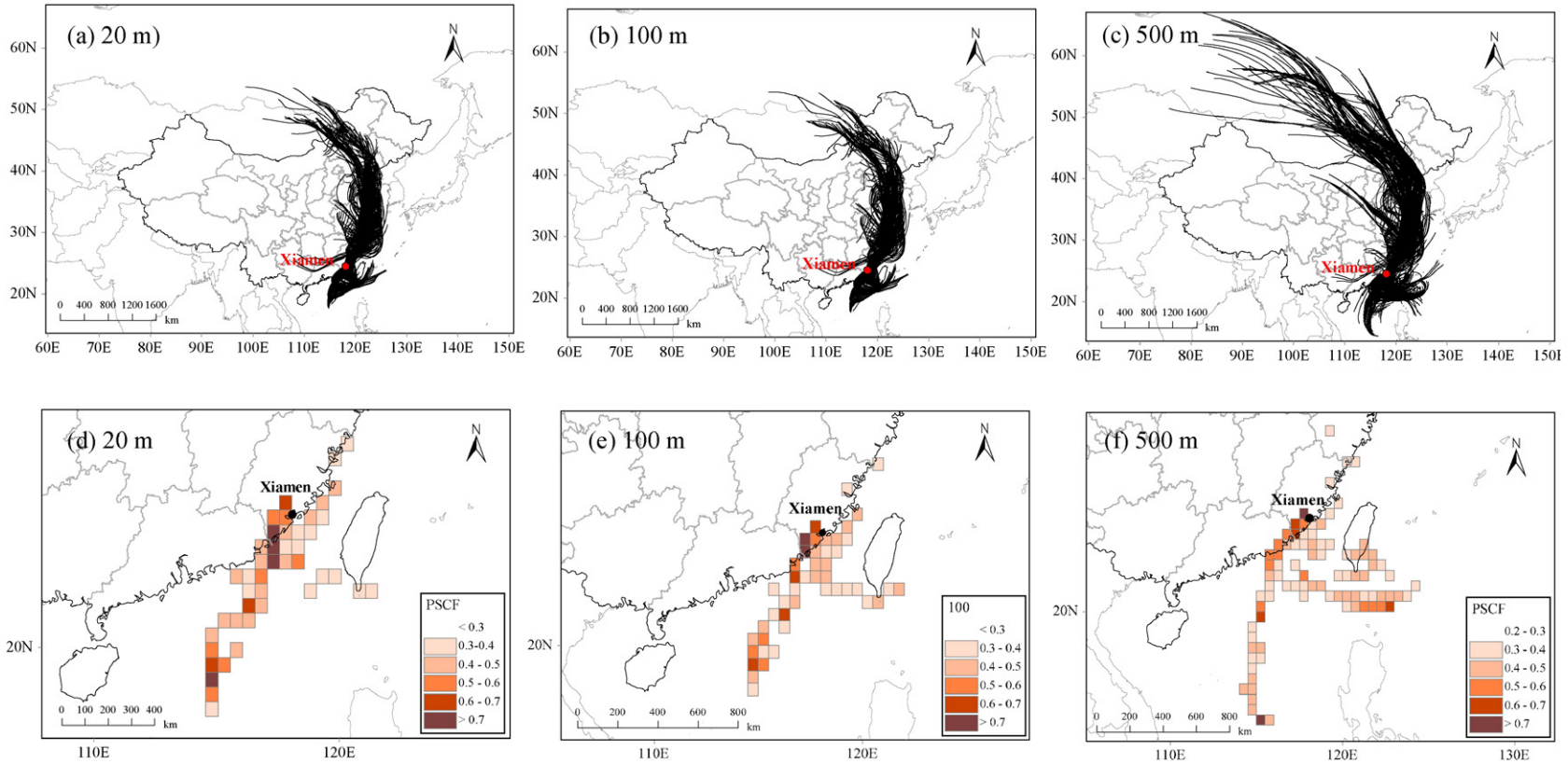

Fig. 4. (a–c) Three-day backward in time air mass trajectories reaching the sampling site at Xiamen at 20, 100, and 500 m above ground every hour and (d–f) likely source areas for rBC during the campaign identified using potential source contribution function (PSCF) model.

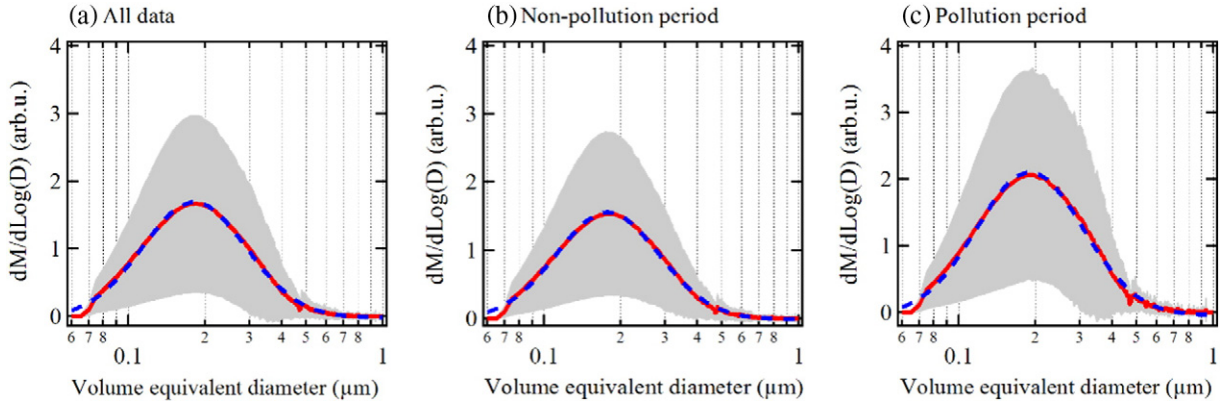

Fig. 5. Mass size distributions of refractory black carbon for (a) the entire campaign period, (b) non-polluted periods ($PM_{2.5} < 75\ \mu g\ m^{-3}$), and (c) polluted periods ($PM_{2.5} > 75\ \mu g\ m^{-3}$). The solid red lines represent average values, the grey shaded region shows the averages ± one standard deviation, and the dashed blue lines are the mono-modal lognormal fits to the data.

2015a), but it falls within the range of 174–193 nm (the diameters were adjusted for comparison by assuming the same density of 2 g cm^{-3} used in our study) reported for various continental sites in Europe (McMeeking et al., 2010).

A single lognormal function fit the data well for the two different levels of $PM_{2.5}$ mass found for the non-polluted and polluted samples (Fig. 5b and c). The rBC MMD for non-polluted samples was ~175 nm ($\sigma_{gc} = 0.46$), which was ~20 nm smaller than for the corresponding value for the polluted ones (~195 nm, $\sigma_{gc} = 0.48$). There is good evidence that the sizes of rBC cores can vary at the time of emission depending on their source, and this affects their ambient size distributions. For example, Liu et al. (2014) reported that rBC particles from solid fuel burning have larger MMDs compared with those from motor vehicles. Analyses of mass spectra of biomass burning particles showed that m/z 60 is a common fragment found in those emissions (Elser et al., 2016), and therefore, the relative abundance of m/z 60 in total organic aerosol (f_{60}) obtained in our studies with the ACSM was used as a chemical tracer of biomass burning. As shown in Fig. S4, the rBC concentration was moderately correlated ($r = 0.65$) with f_{60}, and the latter also was positively correlated with the $PM_{2.5}$ mass concentration ($r = 0.67$). These correlations indicate that the biomass burning was an important source, contributing to both the increased $PM_{2.5}$ and rBC loadings during pollution episodes.

Previous studies indicate that the rBC MMD for particles from biomass burning plume (210 nm) was larger than that from urban fossil fuel burning (170 nm) (Schwarz et al., 2008a). Thus, the larger rBC size during pollution episodes also was likely connected to the enhanced biomass burning activities. In addition, one may also postulate that the increased rBC core size could result from coagulation processes. It bears repeating that the SP2 quantifies the mass of the rBC core alone, and it does not account for any contributions of non-rBC material to the rBC particle diameter. However, the self-coagulation of rBC particles in the atmosphere is mainly the result Brownian motion, which is a slow process for particles in the accumulation mode (Seinfeld and Pandis, 2006). It is possible that the ageing scale may not be long enough to lead to a significant increase in rBC core during pollution episodes.

3.3. The rBC mixing state and relationships with chemical species

The mixing state of rBC aerosol is one of the most critical parameters used in models that deal with the direct radiative forcing of aerosols (Bond et al., 2013). A time-series plot of the hourly-averaged mixing state of rBC particles (expressed as a percentage, f_{BC}) for the entire campaign is shown in Fig. 2b. The f_{BC} results can be viewed as indicator of the relative proportions of fresh emissions versus aged particles. In our study, f_{BC} varied over a range of 18–55%, with an average value of 31 ± 6%, suggesting that the bulk of the rBC aerosol was either uncoated or thinly-coated. This value was lower than SP2-based measurements reported for other Chinese cities, e.g., 58% at Beijing (Wu et al., 2016) and 47% at Xi'an (Wang et al., 2014a), and a remote area of Qinghai Lake (59%, Wang et al., 2015b).

Fig. 6 shows the diurnal variations of f_{BC} and oxidant levels ($Ox = O_3 + NO_2$) averaged over the study. The oxidant Ox is a more conserved tracer of photochemical processing in the urban atmosphere than O_3 alone because fresh emissions of NO can react with O_3 to form NO_2 (Notario et al., 2012). The diurnal pattern in f_{BC} was roughly opposite that shown by the rBC concentrations; that is, low f_{BC} values were found in the early morning and evening, which can be attributed to

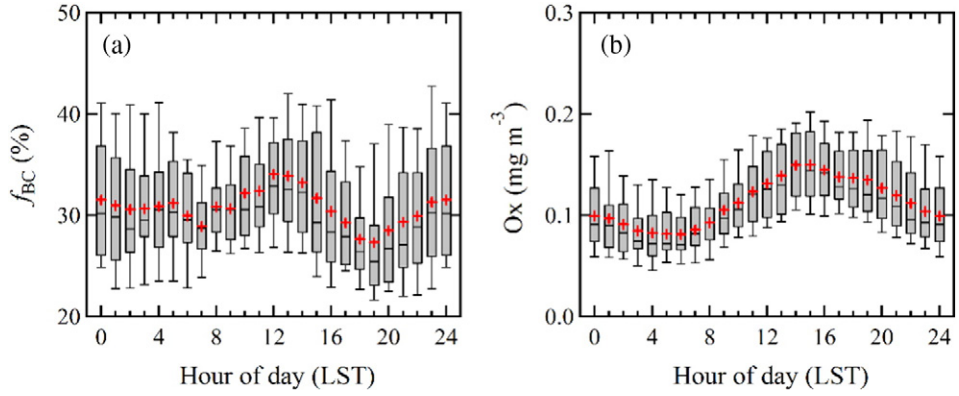

Fig. 6. (a) Diurnal variations of the number fraction of thickly-coated rBC particles (f_{BC}) and (b) oxidant Ox ($O_3 + NO_2$) concentrations averaged over the study. Boxes and whiskers as in Fig. 3.

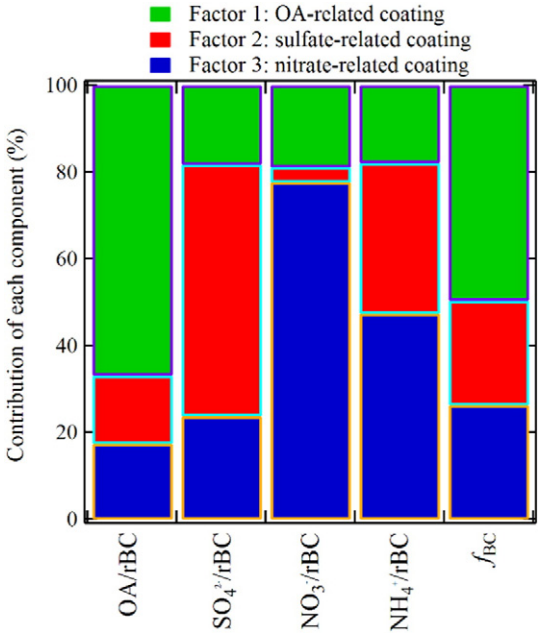

Fig. 7. Contributions of organic aerosol (OA) and major ions normalized to rBC (OA/rBC, SO_4^{2-}/rBC, NO_3^-/rBC, NH_4^+/rBC), and f_{BC} for the three-factor positive matrix factorization (PMF) model for the rBC coatings.

the production of fresh, externally-mixed rBC particles by motor vehicles. An increase in f_{BC} was observed from 09:00 to 14:00, which was followed by the increase in Ox (Fig. 6b). The greater numbers of coated rBC particles during the daytime are an indication that photochemical oxidation plays an important role in the evolution of the rBC mixing state at our site. Moreover, deeper mixed-layers and higher wind speeds in the afternoon would bring more aged air (that is, regional outflow and/or upper atmospheric air) to the sampling site, and that aged air would tend to contain higher proportions of internally mixed rBC particles (Schwarz et al., 2008b). An increasing trend of f_{BC} was found between 20:00 and 24:00, and one possible explanation for the higher fraction of coated particles at that time is that more aged air from northeast was sampled due to the slightly higher wind speeds in the late evening. Another explanation is that the fresh, externally-mixed rBC particles accumulated during evening rush hour and aged locally during the evening.

Previous studies have used positive matrix factorization (PMF) models to evaluate the potential contributions of organic aerosol (OA), sulfate, nitrate, and ammonium to the coatings on rBC particles (Shiraiwa et al., 2007, Metcalf et al., 2012; Wang et al., 2014a). More detailed information concerning the key principles of the PMF approach may be found in the Supplementary Material. The input parameters for the model were the f_{BC} values and the ACSM species' masses normalized by rBC mass. The latter were used in preference to the absolute mass concentrations for each species because the mass ratios have been shown to better represent the relative amounts of materials coating the rBC particles than the concentrations themselves (Shiraiwa et al., 2007). The US EPA PMF 3.0 version was used for our study, and the optimal number of factors was chosen after the analyzing the goodness of Q-values, the scaled residual matrices, G-space plots, the regression diagnostics, and physical meaningfulness of the factor profiles and contributions. A summary of the PMF model performance statistics is reported in Supplementary Table S1. Three coating-related sources were identified as shown in Fig. 7. Factor 1 was characterized by high loadings for OA/rBC, and it was ascribed to an OA-related coating source. Factor 2 was dominated by SO_4^{2-}/rBC and NH_4^+/rBC, and it was interpreted as sulfate-related coating source, most likely involving reactions of ammonia with sulfuric acid or ammonium bisulfate. Factor 3 was most heavily loaded with NO_3^-/rBC and NH_4^+/rBC, and it was considered a nitrate-related coating source.

A multiple linear regression analysis was next used to calculate the hourly contribution of each of the three coating factors to f_{BC}. The samples were separated into polluted versus non-polluted groups based on the $PM_{2.5}$ mass concentrations to investigate the contributions of each coating factor to f_{BC} for the different conditions (see Section 3.1 for classification criteria). Fig. 8 shows the contributions of each of the three factors to f_{BC} during the entire campaign as well as the f_{BC} values separated by the $PM_{2.5}$ levels. On average, Factor 1 contributed 49.5% to f_{BC} over the course of the study, and this indicates that OA was the most important component of the rBC coatings. The combined contributions of Factors 2 and 3 were comparable to the OA loading and accounted for 25.4% and 25.1% of the total coatings, respectively. Closer inspection of the data shows that the coatings on rBC particles varied with the $PM_{2.5}$ mass loadings; that is, the OA coatings (Factor 1) decreased from 51.4% for the non-polluted samples to 42.9% for the polluted ones while the nitrate coatings (Factor 3) showed the opposite behavior and increased from 22.3% to 35.7%. The contribution of sulfate coatings (Factor 2) remained relatively stable under the different $PM_{2.5}$ levels. Previous studies have shown that increases in rBC hydrophilicity were more associated with nitrate coatings than those of sulfate or organic (Liu et al., 2013). Therefore, the increases in the nitrate coatings we observed on rBC from polluted air presumably enhanced the hydrophilicity of the particles, and one possible implication of this is that the

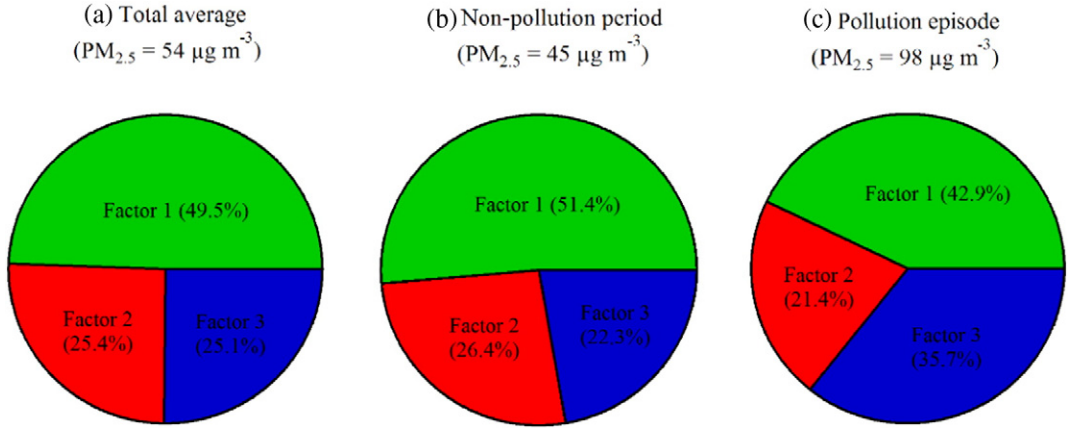

Fig. 8. Contributions of each PMF factor to f_{BC} for (a) the entire campaign period, (b) non-polluted periods, and (c) polluted periods. Factors 1, 2, and 3 represent OA-, sulfate- and nitrate-related coatings, respectively.

atmospheric lifetime of rBC in polluted air could be reduced due to more efficient wet removal.

4. Conclusions

The rBC mass concentrations, size distributions, and mixing state were studied for samples collected from Xiamen, a coastal city in South China. The rBC concentration, averaged over the entire sampling campaign, was 2.3 ± 1.7 μg m^{-3}, which accounted for ~4.3% of $PM_{2.5}$ mass. A clear diurnal cycle in rBC was observed: the concentrations peaked during the morning rush hour, fell to a minimum in the afternoon, then rose again as the traffic increased during the evening, and finally stabilized at night. A potential source contribution function model indicated that the most likely regional sources for rBC were to the southwest of Xiamen, but there were also possible maritime influences due to the heavy commercial shipping traffic. The rBC mass size distribution was approximately lognormal, and the rBC mass median diameter was ~185 nm. The MMD for the polluted samples was larger (~195 nm) than that for the non-polluted samples (~175 nm), which was attributed to a greater impact of biomass burning during polluted conditions.

The average number fraction of thickly-coated rBC (f_{BC}) for the study was 31 ± 6%, and therefore uncoated or thinly-coated rBC particles composed the bulk of the rBC aerosol. Higher f_{BC} values–that is, more thickly-coated particles–were observed in the afternoon evidently due to the effects of photochemical oxidation. Positive matrix factorization model simulations showed that organic substances were the most important materials contributing to the rBC coatings. The organic aerosol coatings were higher in the non-polluted samples than in the polluted ones, 51.4% versus 42.9%, while nitrate coatings made up 35.7% of the coatings for the polluted samples compared with 22.3% for the non-polluted ones. Internal mixing with nitrate presumably makes the rBC particles more hydrophilic, and that could lead to a shorter atmospheric lifetime for rBC in regionally polluted air masses.

Acknowledgements

This work was supported by a project from Ministry of Science and Technology (2013FY112700).

Appendix A. Supplementary data

Supplementary data to this article can be found online at http://dx.doi.org/10.1016/j.atmosres.2016.06.022.

References

Bond, T.C., Doherty, S.J., Fahey, D.W., Forster, P.M., Berntsen, T., DeAngelo, B.J., Flanner, M.G., Ghan, S., Kaercher, B., Koch, D., Kinne, S., Kondo, Y., Quinn, P.K., Sarofim, M.C., Schultz, M.G., Schulz, M., Venkataraman, C., Zhang, H., Zhang, S., Bellouin, N., Guttikunda, S.K., Hopke, P.K., Jacobson, M.Z., Kaiser, J.W., Klimont, Z., Lohmann, U., Schwarz, J.P., Shindell, D., Storelvmo, T., Warren, S.G., Zender, C.S., 2013. Bounding the role of black carbon in the climate system: a scientific assessment. J. Geophys. Res. 118, 5380–5552.

Cao, J.-J., Zhu, C.-S., Tie, X.-X., Geng, F.-H., Xu, H.-M., Ho, S., Wang, G.-H., Han, Y.-M., Ho, K.-F., 2013. Characteristics and sources of carbonaceous aerosols from Shanghai. China Atmos. Chem. Phys. 13, 803–817.

Cao, J., Zhu, C., Ho, K., Han, Y., Shen, Z., Zhan, C., Zhang, J., 2015. Light attenuation cross-section of black carbon in an urban atmosphere in northern China. Particuology 18, 89–95.

Cape, J.N., Coyle, M., Dumitrean, P., 2012. The atmospheric lifetime of black carbon. Atmos. Environ. 59, 256–263.

Cheng, M.D., Lin, C.J., 2001. Receptor modeling for smoke of 1998 biomass burning in central America. J. Geophys. Res. 106 (D19), 22871–22886.

Cheng, Y.F., Eichler, H., Wiedensohler, A., Heintzenberg, J., Zhang, Y.H., Hu, M., Herrmann, H., Zeng, L.M., Liu, S., Gnauk, T., Brüggemann, E., He, L.Y., 2006. Mixing state of elemental carbon and non-light-absorbing aerosol components derived from in situ particle optical properties at Xinken in Pearl River Delta of China. J. Geophys. Res. 111, D20204. http://dx.doi.org/10.1029/2005JD006929.

Cornell, A.G., Chillrud, S.N., Mellins, R.B., Acosta, L.M., Miller, R.L., Quinn, J.W., Yan, B., Divjan, A., Olmedo, O.E., Lopez-Pintado, S., Kinney, P.L., Perera, F.P., Jacobson, J.S., Goldstein, I.F., Rundle, A.G., Perzanowski, M.S., 2012. Domestic airborne black carbon and exhaled nitric oxide in children in NYC. J. Expo. Sci. Environ. Epidemiol. 22, 258–266.

Cross, E.S., Onasch, T.B., Ahern, A., Wrobel, W., Slowik, J.G., Olfert, J., Lack, D.A., Massoli, P., Cappa, C.D., Schwarz, J.P., Spackman, J.R., Fahey, D.W., Sedlacek, A., Trimborn, A., Jayne, J.T., Freedman, A., Williams, L.R., Ng, N.L., Mazzoleni, C., Dubey, M., Brem, B., Kok, G., Subramanian, R., Freitag, S., Clarke, A., Thornhill, D., Marr, L.C., Kolb, C.E., Worsnop, D.R., Davidovits, P., 2010. Soot particle studies–instrument inter-comparison–project overview. Aerosol Sci. Technol. 44, 592–611.

Das, S.K., Jayaraman, A., 2011. Role of black carbon in aerosol properties and radiative forcing over western India during premonsoon period. Atmos. Res. 102, 320–334.

Draxler, R.R., Rolph, G.D., 2003. HYSPLIT (HYbrid Single-Particle Lagrangian Integrated Trajectory) Model access via NOAA ARL READY Website. http://www.arl.noaa.gov/ready/hysplit4.htmlNOAA Air Resources Laboratory, Silver Spring, MD.

Dumka, U.C., Moorthy, K.K., Kumar, R., Hegde, P., Sagar, R., Pant, P., Singh, N., Babu, S.S., 2010. Characteristics of aerosol black carbon mass concentration over a high altitude location in the central Himalayas from multi-year measurements. Atmos. Res. 96, 510–521.

Elser, M., Huang, R.J., Wolf, R., Slowik, J.G., Wang, Q., Canonaco, F., Li, G., Bozzetti, C., Daellenbach, K.R., Huang, Y., Zhang, R., Li, Z., Cao, J., Baltensperger, U., El-Haddad, I., Prévôt, A.S.H., 2016. New insights into $PM_{2.5}$ chemical composition and sources in two major cities in China during extreme haze events using aerosol mass spectrometry. Atmos. Chem. Phys. 16, 3207–3225.

Feng, J., Zhong, M., Xu, B., Du, Y., Wu, M., Wang, H., Chen, C., 2014. Concentrations, seasonal and diurnal variations of black carbon in $PM_{2.5}$ in Shanghai. China Atmos. Res. 147–148, 1–9.

Gao, R.S., Schwarz, J.P., Kelly, K.K., Fahey, D.W., Watts, L.A., Thompson, T.L., Spackman, J.R., Slowik, J.G., Cross, E.S., Han, J.-H., Davidovits, P., Onasch, T.B., Worsnop, D.R., 2007. A novel method for estimating light-scattering properties of soot aerosols using a modified single-particle soot photometer. Aerosol Sci. Technol. 41, 125–135.

Gong, X., Zhang, C., Chen, H., Nizkorodov, S.A., Chen, J., Yang, X., 2016. Size distribution and mixing state of black carbon particles during a heavy air pollution episode in Shanghai. Atmos. Chem. Phys. 16, 5399–5411.

Hadley, O.L., Kirchstetter, T.W., 2012. Black-carbon reduction of snow albedo. Nat. Clim. Chang. 2, 437–440.

Han, Y.M., Cao, J.J., Lee, S.C., Ho, K.F., An, Z.S., 2010. Different characteristics of char and soot in the atmosphere and their ratio as an indicator for source identification in Xi'an. China Atmos. Chem. Phys. 10, 595–607.

Heal, M.R., Kumar, P., Harrison, R.M., 2012. Particles, air quality, policy and health. Chem. Soc. Rev. 41, 6606–6630.

Huang, X.-F., Sun, T.-L., Zeng, L.-W., Yu, G.-H., Luan, S.-J., 2012. Black carbon aerosol characterization in a coastal city in South China using a single particle soot photometer. Atmos. Environ. 51, 21–28.

IPCC, 2013. Climate Change 2013: The Physical Science Basis. Cambridge University Press, Cambridge, United Kingdom and New York, NY, USA.

Kondo, Y., Sahu, L., Moteki, N., Khan, F., Takegawa, N., Liu, X., Koike, M., Miyakawa, T., 2011. Consistency and traceability of black carbon measurements made by laser-induced incandescence, thermal-optical transmittance, and filter-based photo-absorption techniques. Aerosol Sci. Technol. 45, 295–312.

Laborde, M., Crippa, M., Tritscher, T., Jurányi, Z., Decarlo, P.F., Temime-Roussel, B., Marchand, N., Eckhardt, S., Stohl, A., Baltensperger, U., Prévôt, A.S.H., Weingartner, E., Gysel, M., 2013. Black carbon physical properties and mixing state in the European megacity Paris. Atmos. Chem. Phys. 13, 5831–5856.

Lack, D.A., Corbett, J.J., 2012. Black carbon from ships: a review of the effects of ship speed, fuel quality and exhaust gas scrubbing. Atmos. Chem. Phys. 12, 3985–4000.

Li, W.J., Zhang, D.Z., Shao, L.Y., Zhou, S.Z., Wang, W.X., 2011. Individual particle analysis of aerosols collected under haze and non-haze conditions at a high-elevation mountain site in the North China plain. Atmos. Chem. Phys. 11, 11733–11744.

Liu, D., Allan, J., Whitehead, J., Young, D., Flynn, M., Coe, H., McFiggans, G., Fleming, Z.L., Bandy, B., 2013. Ambient black carbon particle hygroscopic properties controlled by mixing state and composition. Atmos. Chem. Phys. 13, 2015–2029.

Liu, D., Allan, J.D., Young, D.E., Coe, H., Beddows, D., Fleming, Z.L., Flynn, M.J., Gallagher, M.W., Harrison, R.M., Lee, J., Prevot, A.S.H., Taylor, J.W., Yin, J., Williams, P.I., Zotter, P., 2014. Size distribution, mixing state and source apportionment of black carbon aerosol in London during wintertime. Atmos. Chem. Phys. 14, 10061–10084.

Liu, S., Aiken, A.C., Gorkowski, K., Dubey, M.K., Cappa, C.D., Williams, L.R., Herndon, S.C., Massoli, P., Fortner, E.C., Chhabra, P.S., Brooks, W.A., Onasch, T.B., Jayne, J.T., Worsnop, D.R., China, S., Sharma, N., Mazzoleni, C., Xu, L., Ng, N.L., Liu, D., Allan, J.D., Lee, D., Fleming, Z., Mohr, C., Zotter, P., Szidat, S., Prévôt, A.S.H., 2015. Enhanced light absorption by mixed source black and brown carbon particles in UK winter. Nat. Commun. 6. http://dx.doi.org/10.1038/ncomms9435.

McMeeking, G.R., Hamburger, T., Liu, D., Flynn, M., Morgan, W.T., Northway, M., Highwood, E.J., Krejci, R., Allan, J.D., Minikin, A., Coe, H., 2010. Black carbon measurements in the boundary layer over western and northern Europe. Atmos. Chem. Phys. 10, 9393–9414.

Metcalf, A.R., Craven, J.S., Ensberg, J.J., Brioude, J., Angevine, W., Sorooshian, A., Duing, H.T., Jonsson, H.H., Flagan, R.C., Seinfeld, J.H., 2012. Black carbon aerosol over the Los Angeles Basin during CalNex. J. Geophys. Res. 117. http://dx.doi.org/10.1029/2011JD017255.

Middlebrook, A.M., Bahreini, R., Jimenez, J.L., Canagaratna, M.R., 2012. Evaluation of composition-dependent collection efficiencies for the aerodyne aerosol mass spectrometer using field data. Aerosol Sci. Technol. 46, 258–271.

Moteki, N., Kondo, Y., Miyazaki, Y., Takegawa, N., Komazaki, Y., Kurata, G., Shirai, T., Blake, D., Miyakawa, T., Koike, M., 2007. Evolution of mixing state of black carbon particles: aircraft measurements over the western Pacific in March 2004. Geophys. Res. Lett. 34, L11803. http://dx.doi.org/10.1029/2006GL028943.

Ng, N.L., Herndon, S.C., Trimborn, A., Canagaratna, M.R., Croteau, P.L., Onasch, T.B., Sueper, D., Worsnop, D.R., Zhang, Q., Sun, Y.L., Jayne, J.T., 2011. An aerosol chemical speciation

monitor (ACSM) for routine monitoring of the composition and mass concentrations of ambient aerosol. Aerosol Sci. Technol. 45, 780–794.
Ni, M., Huang, J., Lu, S., Li, X., Yan, J., Cen, K., 2014. A review on black carbon emissions, worldwide and in China. Chemosphere 107, 83–93.
Notario, A., Bravo, I., Adame, J.A., Díaz-de-Mera, Y., Aranda, A., Rodríguez, A., Rodríguez, D., 2012. Analysis of NO, NO, NOx, O_3 and oxidant ($OX = O_3 + NO_2$) levels measured in a metropolitan area in the southwest of Iberian peninsula. Atmos. Res. 104, 217–226.
Perring, A.E., Schwarz, J.P., Spackman, J.R., Bahreini, R., de Gouw, J.A., Gao, R.S., Holloway, J.S., Lack, D.A., Langridge, J.M., Peischl, J., Middlebrook, A.M., Ryerson, T.B., Warneke, C., Watts, L.A., Fahey, D.W., 2011. Characteristics of black carbon aerosol from a surface oil burn during the Deepwater Horizon oil spill. Geophys. Res. Lett. 38, L17809. http://dx.doi.org/10.1029/2011GL048356.
Petzold, A., Ogren, J.A., Fiebig, M., Laj, P., Li, S.M., Baltensperger, U., Holzer-Popp, T., Kinne, S., Pappalardo, G., Sugimoto, N., Wehrli, C., Wiedensohler, A., Zhang, X.Y., 2013. Recommendations for reporting "black carbon" measurements. Atmos. Chem. Phys. 13, 8365–8379.
Ramana, M.V., Ramanathan, V., Feng, Y., Yoon, S.-C., Kim, S.-W., Carmichael, G.R., Schauer, J.J., 2010. Warming influenced by the ratio of black carbon to sulphate and the black-carbon source. Nat. Geosci. 3, 542–545.
Ramanathan, V., Carmichael, G., 2008. Global and regional climate changes due to black carbon. Nat. Geosci. 1, 221–227.
Reddington, C.L., McMeeking, G., Mann, G.W., Coe, H., Frontoso, M.G., Liu, D., Flynn, M., Spracklen, D.V., Carslaw, K.S., 2013. The mass and number size distributions of black carbon aerosol over Europe. Atmos. Chem. Phys. 13, 4917–4939.
Schwarz, J.P., Gao, R.S., Fahey, D.W., Thomson, D.S., Watts, L.A., Wilson, J.C., Reeves, J.M., Darbeheshti, M., Baumgardner, D.G., Kok, G.L., Chung, S.H., Schulz, M., Hendricks, J., Lauer, A., Kärcher, B., Slowik, J.G., Rosenlof, K.H., Thompaon, T.L., Langford, A.O., Loewenstein, M., Aikin, K.C., 2006. Single-particle measurements of midlatitude black carbon and light-scattering aerosols from the boundary layer to the lower stratosphere. J. Geophys. Res. 111, D16207. http://dx.doi.org/10.1029/2006JD007076.
Schwarz, J., Gao, R., Spackman, J., Watts, L., Thomson, D., Fahey, D., Ryerson, T., Peischl, J., Holloway, J., Trainer, M., Frost, G.J., Baynard, T., Lack, D.A., de Gouw, J.A., Warneke, C., Negro, L.A.D., 2008a. Measurement of the mixing state, mass, and optical size of individual black carbon particles in urban and biomass burning emissions. Geophys. Res. Lett. 35, L13810. http://dx.doi.org/10.1029/2008GL033968.
Schwarz, J.P., Spackman, J.R., Fahey, D.W., Gao, R.S., Lohmann, U., Stier, P., Watts, L.A., Thomson, D.S., Lack, D.A., Pfister, L., Mahoney, M.J., Baumgardner, D., Wilson, J.C., Reeves, J.M., 2008b. Coatings and their enhancement of black carbon light absorption in the tropical atmosphere. J. Geophys. Res. 113, D03203. http://dx.doi.org/10.1029/2007JD009042.
Schwarz, J.P., Spackman, J.R., Gao, R.S., Perring, A.E., Cross, E., Onasch, T.B., Ahern, A., Wrobel, W., Davidovits, P., Olfert, J., Dubey, M.K., Mazzoleni, C., Fahey, D.W., 2010. The detection efficiency of the single particle soot photometer. Aerosol Sci. Technol. 44, 612–628.
Schwarz, J.P., Perring, A.E., Markovic, M.Z., Gao, R.S., Ohata, S., Langridge, J., Law, D., McLaughlin, R., Fahey, D.W., 2015. Technique and theoretical approach for quantifying the hygroscopicity of black-carbon-containing aerosol using a single particle soot photometer. J. Aerosol Sci. 81, 110–126.
Seinfeld, J.H., Pandis, S.N., 2006. Atmospheric Chemistry and Physics: From Air Pollution to Climate Change. second ed. John Wiley & Sons, New York.
Shiraiwa, M., Kondo, Y., Moteki, N., Takegawa, N., Miyazaki, Y., Blake, D.R., 2007. Evolution of mixing state of black carbon in polluted air from Tokyo. Geophys. Res. Lett. 34, L16803. http://dx.doi.org/10.1029/2007GL029819.
Slowik, J.G., Stainken, K., Davidovits, P., Williams, L.R., Jayne, J.T., Kolb, C.E., Worsnop, D.R., Rudich, Y., DeCarlo, P.F., Jimenez, J.L., 2004. Particle morphology and density characterization by combined mobility and aerodynamic diameter measurements. Part 2: application to combustion-generated soot aerosols as a function of fuel equivalence ratio. Aerosol. Sci. Technol. 38, 1206–1222.
Wang, Q., Cao, J., Tao, J., Li, N., Su, X., Chen, L.W.A., Wang, P., Shen, Z., Liu, S., Dai, W., 2013. Long-term trends in visibility and at Chengdu, China. PLoS One 8 (7), e68894. http://dx.doi.org/10.1371/journal.pone.0068894.
Wang, Q., Huang, R.-J., Cao, J., Han, Y., Wang, G., Li, G., Wang, Y., Dai, W., Zhang, R., Zhou, Y., 2014a. Mixing state of black carbon aerosol in a heavily polluted urban area of China: implications for light absorption enhancement. Aerosol Sci. Technol. 48, 689–697.
Wang, Q., Schwarz, J.P., Cao, J., Gao, R., Fahey, D.W., Hu, T., Huang, R.-J., Han, Y., Shen, Z., 2014b. Black carbon aerosol characterization in a remote area of Qinghai–Tibetan plateau, western China. Sci. Total Environ. 479, 151–158.
Wang, Q., Liu, S., Zhou, Y., Cao, J., Han, Y., Ni, H., Zhang, N., Huang, R., 2015a. Characteristics of black carbon aerosol during the Chinese lunar year and weekdays in Xi'an, China. Atmosphere 6, 195–208.
Wang, Q.Y., Huang, R.J., Cao, J.J., Tie, X.X., Ni, H.Y., Zhou, Y.Q., Han, Y.M., Hu, T.F., Zhu, C.S., Feng, T., Li, N., Li, J.D., 2015b. Black carbon aerosol in winter northeastern Qinghai-Tibetan plateau, China: the source, mixing state and optical property. Atmos. Chem. Phys. 15, 13059–13069.
Wang, R., 2015. Global Emissions of Black Carbon From 1960 to 2007, Global Emission Inventory and Atmospheric Transport of Black Carbon. Springer, pp. 115–129.
Wu, D., Wu, C., Liao, B., Chen, H., Wu, M., Li, F., Tan, H., Deng, T., Li, H., Jiang, D., Yu, J.Z., 2013. Black carbon over the South China Sea and in various continental locations in South China. Atmos. Chem. Phys. 13, 12257–12270.
Wu, Y., Zhang, R., Tian, P., Tao, J., Hsu, S.-C., Yan, P., Wang, Q., Cao, J., Zhang, X., Xia, X., 2016. Effect of ambient humidity on the light absorption amplification of black carbon in Beijing during January 2013. Atmos. Environ. 124, 217–223.
Xu, B., Cao, J., Hansen, J., Yao, T., Joswia, D.R., Wang, N., Wu, G., Wang, M., Zhao, H., Yang, W., 2009. Black soot and the survival of Tibetan glaciers. P. Natl. Acad. Sci. USA 106, 22114–22118.
Zhang, D., Zhang, R., 2005. Laboratory investigation of heterogeneous interaction of sulfuric acid with soot. Environ. Sci. Technol. 39, 5722–5728.
Zhang, Q., Streets, D.G., Carmichael, G.R., He, K.B., Huo, H., Kannari, A., Klimont, Z., Park, I.S., Reddy, S., Fu, J.S., Chen, D., Duan, L., Lei, Y., Wang, L.T., Yao, Z.L., 2009. Asian emissions in 2006 for the NASA INTEX-B mission. Atmos. Chem. Phys. 9, 5131–5153.
Zhang, R., Jing, J., Tao, J., Hsu, S.-C., Wang, G., Cao, J., Lee, C., Zhu, L., Chen, Z., Zhao, Y., 2013. Chemical characterization and source apportionment of $PM_{2.5}$ in Beijing: seasonal perspective. Atmos. Chem. Phys. 13, 7053–7074.
Zhu, C.-S., Cao, J.-J., Tsai, C.-J., Shen, Z.-X., Han, Y.-M., Liu, S.-X., Zhao, Z.-Z., 2014. Comparison and implications of $PM_{2.5}$ carbon fractions in different environments. Sci. Total Environ. 466, 203–209.